Cancer Nanotechnology

RESEARCH Open Access

# Preparation and characterization of cetuximab-loaded egg serum albumin nanoparticles and their uses as a drug delivery system against Caco-2 colon cancer cells

Elsayed I. Salim[1*], Abeer M. Mosbah[2], F. A. Elhussiny[2], Nemany A. N. Hanafy[3] and Y. Abdou[2]

*Correspondence: elsayed.salim@science.tanta.edu.eg

[1] Department of Zoology, Research Lab. of Molecular Carcinogenesis, Faculty of Science, Tanta University, Tanta 31527, Egypt
[2] Department of Physics, Faculty of Science, Tanta University, Tanta 31527, Egypt
[3] Institute of Nanoscience and Nanotechnology, Kafrelsheikh University, Kafrelsheikh 33516, Egypt

## Abstract

To avoid the harmful side effects of cetuximab and improve its therapeutic efficacy, egg serum albumin (ESA) was used as a targeting drug carrier moiety for cancer therapy against Caco-2 colon cancer cells. The simple improved desolvation method was used to synthesize ESA nanoparticles (ESA-NPs) and cetuximab-loaded albumin nanoparticles (CET-ANPs) with glutaraldehyde as a crosslinking agent. The ESA-NPs and CET-ANPs were spherically shaped, and their sizes and surface potentials were 100 and − 24 nm and 170 and − 20 nm, respectively, as determined using transmission electron microscopy (TEM) and a Zeta potential analyzer. The specific functional groups of the prepared nanoparticles were revealed by FTIR analysis. In the MTT (3-(4, 5-dimethylthiazolyl-2)-2, 5-diphenyltetrazolium bromide) assay, CET-ANPs exerted the highest antitumor activity after 24 h followed by CET, ESA-NPs, and pure ESA. Combination of CET + ESA-NPs at different IC50 concentrations at ratios of 1:1, 1:2, 2:1, 1:4, 4:1, 1:9, or 9:1 showed significant synergistic effects with a combination index (CI) > 1. Furthermore, the CET either loaded with ESA-NPs or administered in combination (CET + ESA NPs) caused significant apoptotic damage, as well as an S-phase or G2/M cell cycle arrest to the cancer cells, respectively. These were directly linked with a significant upregulation of mRNA expression of *Caspase3* and *Bax* genes and an extreme downregulation of the mRNA expression of *Bcl2,* particularly in the combination treatment group, as compared to the untreated cells. Finally, ESA-NPs improved the effectiveness of cetuximab, strongly caused apoptotic and antiproliferative action with lower systemic toxicity, and could be suggested for the targeted administration of anticancer medications in various nanosystems.

**Keywords:** Albumin nanoparticles, Cetuximab, Caco-2 colon cancer cells, Apoptosis, cell cycle arrest

© The Author(s) 2023. **Open Access** This article is licensed under a Creative Commons Attribution 4.0 International License, which permits use, sharing, adaptation, distribution and reproduction in any medium or format, as long as you give appropriate credit to the original author(s) and the source, provide a link to the Creative Commons licence, and indicate if changes were made. The images or other third party material in this article are included in the article's Creative Commons licence, unless indicated otherwise in a credit line to the material. If material is not included in the article's Creative Commons licence and your intended use is not permitted by statutory regulation or exceeds the permitted use, you will need to obtain permission directly from the copyright holder. To view a copy of this licence, visit http://creativecommons.org/licenses/by/4.0/. The Creative Commons Public Domain Dedication waiver (http://creativecommons.org/publicdomain/zero/1.0/) applies to the data made available in this article, unless otherwise stated in a credit line to the data.

## Background

Colorectal cancer (CRC) or colon cancer, is one of the most common forms of cancer among Western people, where estimation of age-standardized rate (ASRs) by Globocan, 2020, (Sung et al. 2021) indicates that colon cancer incidence in both sexes is the fourth among all types of cancer worldwide (ASR incidence: 19.5/100,000), and it has more than 1 million new cases every year (Feng et al. 2017). In Egypt, it was reported previously that females appeared to be at a slightly higher risk of developing colon cancer with a prevalence of 1.2:1 (Abou-Zeid et al. 2002; El-Bolkainy et al. 2006); in more detail, 62.8% of cases had primary colonic lesions in the cases studied by Veruttipong et al. (2012). This situation is currently still the case where females have higher incidence and mortality ASRs of colon cancer than males (Abou-Zeid et al. 2002). Despite recent progress, colon cancer remains the third greatest cause of death among cancer patients worldwide (after lung and female breast cancers) (Sung et al. 2021).

Chemotherapy has great potential for treating cancer patients, but it has a lot of negative side effects on normal tissues (Fogh 1986). Cetuximab is a chimeric monoclonal antibody that targets epidermal growth factor receptors (EGFR) by competitively inhibiting their natural ligands, fostering EGFR internalization, and altering EGFR-dependent signaling in some FDA-approved indications, such as metastatic colorectal cancer with wild-type *KRAS* (without mutation), and head and neck cancer (squamous cell). This study aims to fabricate optimal nanoparticles as carriers that can overcome the drawbacks of cetuximab to be used later in cancer therapy while the FDA's unapproved uses for cetuximab mainly include colorectal cancer with *KRAS* mutations, non-small cell lung cancer (NSCLC), EGFR expression, and advanced squamous cell skin cancer, with it having several side effects attributed to its interaction with normal cells, which interaction causes papulopustular rashes (acne-like), whereas xerosis, eczema, fissures, telangiectasia, hyperpigmentation, and nail and hair changes occur less frequently (Štulhofer Buzina et al. 2016).

Albumin is one of the most important and abundant proteins in the body and eggs due to its role in maintaining intravascular colloid osmotic pressure, neutralizing toxins, and transporting therapeutic agents. The main protein found in the egg white is ovalbumin (OVA), representing 55% of the total protein contents, followed by ovotransferrin (12%), ovomucoid (11%), ovoglobulin (4%), ovomucin (3.5%), lysozyme (3.4%), ovomacroglobulin (0.5%), and other less abundant proteins (Karami et al. 2014).

## Methods

### Chemicals

Cetuximab (Erbitux) was purchased from Eli Lilly and Co., Indianapolis, U.S.A. Standard egg serum albumin (ESA) powder with an analytical grade of 95.2% (CAS no.9006–59-1) was obtained from ALPHA CHEMIKA (Bombay- India). PBS tablets of pH = 7.3 were purchased from Oxoid Limited Basingstoke, Hampshire, England.

#### Preparation of cetuximab-loaded ESA nanospheres

To prepare the ESA-NPs, the simple improved desolvation method was used. Briefly, 40 mg ESA was added to 10 mM NaCl. After dissolution, the solution was titrated to

pH = 8.5 with 1 N NaOH and stirred for 5 min. Afterward, 32 mL of 90% ethanol was added until the ESA solution became turbid. Glutaraldehyde (12 µl/mL) was added as a crosslinking agent. Then, the solution was stirred overnight. The nanoparticles were centrifuged thrice and washed with deionized water. To prepare the cetuximab-loaded ESA-Ps (CET-ESA NPs), minor modifications were performed. Briefly, 50 mg ESA was dissolved in 80 ml double distilled water under stirring and sonication for 15 and 10 min, respectively. Afterward, 4 ml of 20 mg CET was diluted in 10 ml of 0.9% saline and further added and mixed with the ESA solution. After 30 min of stirring, 5 ml of absolute ethanol was added, and finally, the CET-loaded ESA-NPs were kept for freeze-drying lyophilization (Ye et al. 2021).

## Characterization

### *Transmission electron microscopy (TEM)*

For the TEM analysis, 1 ml of the prepared NP sample dispersion was diluted with the solvent and sonicated for 5 min. Afterward, a few microliters of the NP solution were placed on standard TEM carbon-coated Cu-grids, and the solvent was allowed to evaporate completely within 15 min before staining with an aqueous solution of phosphotungstic acid. The grid was thoroughly air-dried, and the samples were imaged under a JEOL JEM 2100 TEM microscope operating at 200 kV.

### *Zeta potential and dynamic light scattering (DLS) measurements*

The electrophoretic mobilities of the samples were determined by photon correlation spectroscopy using a Zeta sizer Nano series (Brookhaven Instruments, NY 11,472, U.S.A.). The prepared NP dispersions of 0.1 ml were diluted with 10 ml of double distilled water and mixed well before measuring (Salim et al. 2022). All measurements were performed at 25 °C, and five consecutive measurements were taken for the analysis.

### *UV–Vis spectroscopy and fluorescence spectrophotometry*

The absorbance of samples was measured using a UV visible absorbance spectrophotometer (Jasco V-770). Here, 500 µl of the fabricated assembly was diluted in 4 ml double distilled water and scanned at a range of 200–800 nm. All samples' absorbance was measured by a fluorescence spectrophotometer by the same procedure. The results were analyzed by Origin 8 software (Origin Lab Corporation, Northampton, MA 01,060, U.S.A.).

### *Fourier transform infrared spectroscopy (FTIR)*

A Fourier Transform Infrared Spectrometer (JASCO, JAPAN, model no. AUP1200343), in at least three scans recorded on different regions of the samples, and the representative spectra analyzed, was used to detect the surface molecular structures in the range of 500–4000 $cm^{-1}$ using the KBr pellet method.

### *Determination of loading capacity and loading efficiency*

To determine the drug-loading capacity within the synthesized nanoparticles, 10 mg of cetuximab-loaded albumin nanoparticles (CET-ANPs) were dissolved in 10 mL of double distilled water. After homogenous melting, the solution was centrifuged at 4500×*g*

for 20 min and then the resulting pellet of cetuximab was lyophilized. Equal concentrations of empty (non-loaded) NPs (ESA-NPs) were prepared, collected after centrifugation, and lyophilized (Ali et al. 2018). The total amount of drug loaded onto the NPs was calculated in percentages as described in the following formula:

$$\text{The encapsulation efficiency (EE \%)} = \text{weight of loaded cetuximab/weight of initially added cetuximab} \times 100, \quad (1)$$

while the loading capacity (LC%) was estimated as follows (Ali et al. 2018; Hanafy et al. 2020):

$$\text{Weight of loaded cetuximab/total weight of NPs without cetuximab} \times 100. \quad (2)$$

#### *SDS-PAGE*

SDS-PAGE was used to confirm the presence of bands of the pure ESA, pure CET, and ESA-NPs, and to ensure the CET loading on CET-ANPs. A vertical electrophoresis system (MiniVE, Hoefer, U.S.A.) was used at a 75-V constant voltage for 30 min, then 115 V for 1.5 h in electrophoresis buffer (0.25 mM Tris, 1.92 mM glycine, 1% SDS, and pH = 8.3). The gel was stained with Coomassie brilliant blue buffer for 1 h and washed with a destaining agent (40% methanol, 7% acetic acid, and 53% water) (Khaliq et al. 2021).

### Cell viability by MTT assay

To assess the effects of serial concentrations of 0, 12.5, 25, 50, 100, and 200 µg/ml of the pure ESA and pure CET, as well as the effect of ESA-NPs, CET-ESA NPs, or the combination of CET + ESA-NPs on the tumor cell growth, the cell viability of Caco-2 colon cancer cells was evaluated by MTT assay (Sigma-Aldrich Inc., St. Louis, MO, USA). This assay is based on a mitochondrial-dependent reduction of the yellow MTT to purple formazan. Briefly, after 24 h of the drug exposure to cells at 200 µg/ml, a 5 mg/ml MTT reagent was added to each well, and the reaction was allowed to proceed for 3–4 h at 37 °C. Afterward, the culture medium was removed and precipitated formazan crystals were dissolved by adding 200 µl DMSO. The absorbance of each well was read using a microplate multiwell reader at 570 nm, which is directly correlated to the number of remaining viable cells. The absorbance data were normalized to the percentage of the vehicle-treated control and graphed afterward. The results were used to calculate the IC50 values of each drug or NPs using the probit analysis (SPSS, ver. 22, SPSS Incorp., Chicago, U.S.A).

#### *Combination therapy bioassay*

After calculating the IC50 levels for each treatment compound, a CET + ESA-NPs combination of cetuximab (IC50) and ESA-NPs (IC50) was applied as a treatment for Caco-2 cells at ratios of 1:1, 1:2, 2:1, 1:4, 4:1, 1:9, and 9:1, respectively (Khamis et al. 2018). All combination treatments were made using fractions of IC50 of CET and ESA-NPs in a nonconstant ratio. Compared to a single-drug therapy, the top combination for the cell line with the lowest CET dosages and combination index (CI) and the maximum cell

death were chosen for additional molecular research. All treatments were administered to 70%–80% confluent Caco-2 cells, which were immediately processed for molecular and flow cytometric analyses after being subsequently cultured in a $CO_2$ incubator for 24 h before being collected by trypsinization.

#### *CI analysis*

To study the drug–drug interaction level between the different combinations of the CET and ESA-NPs against Caco-2 cells, the CI was calculated using the data obtained from their MTT assays. This drug combination study was based on the concentration-effect curves generated as a plot of the fraction of unaffected cells vs. drug concentration by Chou and Talalay (1984) approach, applied to CompuSyn software (PD Science, LLC, USA). The CI values indicate synergistic, antagonistic, and additive effects when $<, >$, and $= 1$, respectively.

### Flow cytometry

#### *Annexin V-FITC apoptosis detection by flow cytometry*

The percentages of cell death apoptosis and necrosis were investigated using the Annexin V-FITC apoptosis detection kit (Abcam Inc., Cambridge Science Park, Cambridge, UK) in response to the efficacy of pure ESA, CET, ESA-NPs, CET-ESA NPs, and CET + ESA-NPs (Ferrado et al. 2020). Briefly, Caco-2 cell lines were exposed to IC50 for 24 h. Afterward, cells were collected and washed twice with PBS of pH = 7.2. Then cells were incubated at 0.5 mL of Annexin V-FITC/ propidium iodide (PI) solution for 30 min in a dark place at room temperature according to the manufacturer's protocol. After staining, cells were injected via ACEA Novocyte™ flow cytometer (ACEA Biosciences Inc., San Diego, CA, USA) and analyzed for FITC and PI fluorescent signals using FL1 and FL2 signal detectors, respectively (λex/emn488/530 nm for FITC and λex/em 535/617 nm for PI). For each sample, 12,000 events were acquired, and positive FITC and/or PI cells were quantified by quadrant analysis and calculated using ACEA NovoExpress™ software (ACEA Biosciences Inc., San Diego, CA, USA).

#### *Cell cycle analysis by flow cytometry*

Caco-2 cells ($10^5$ cells) were collected by trypsinization after their treatment with IC50 of pure ESA, pure CET, ESA-NPs, CET-ANPs, and the combination of CET + ESA-NPs (the most effective doses) for 24 h. Next, the cells were washed twice with ice-cold PBS (pH = 7.4). Afterward, the cells were resuspended in 2 ml of 70% ice-cold ethanol and incubated at 4 °C for 1 h for fixation. The fixed cells were further washed twice with PBS (pH = 7.4) and resuspended in 1 mL PBS containing 50-µg/Ml RNAase A and 10-µg/Ml PI. After 30 min of incubation in a dark place, MCF-7 cells were analyzed for DNA contents by flow cytometry analysis using an FL2 (λex/em 535/617 nm) signal detector (ACEA Novocyte™ flow cytometer, ACEA Biosciences Inc., San Diego, CA, USA). For each sample, 12,000 events were acquired. Cell cycle distribution was calculated using ACEA NovoExpress™ software (ACEA Biosciences Inc., San Diego, CA, USA) (Kis et al. 2022).

### Gene expression analysis by qRT-PCR

The total ribonucleic acid (RNA) was extracted using the Trizol reagent (Invitrogen, Carlsbad, CA) following the manufacturer's protocol (Hatanpaa et al. 2010). Complementary deoxyribonucleic acid (cDNA) was synthesized from the RNA by applying a first-strand cDNA synthesis kit (Fermentas, Vilnius, Lithuania) based on the manufacturer's protocol. The thermocycler for cDNA synthesis was set up at 37 °C for 30 min. The quick PCR (qPCR) was performed using an Applied Biosystems 73Real-Timeime PCR System (Applied Biosystems, Branchburg, NJ, USA) under three conditions: 95 °C for 5 min, 45 cycles at 95 °C for 30 s, and 60 °C for 1 min. The expression levels of mRNA were normalized to the *GAPDH* gene as the endogenous control. Next, the relative differences between the control and treatment groups were calculated and expressed. Primers and probes for the qPCR were designed using Allele ID 6. All primers are presented in Table 1.

### Statistical analysis

The results were expressed as the mean ± the standard division of the mean (SEM). In data representative of at least three independent triplicates, it was analyzed by SPSS, version 20, using one-way analysis of variance, followed by Duncan's test for comparison between the different treatment groups.

## Results

### Characterization of CET-ANPs

#### *TEM*

In the prepared ESA-NPs, the CET was integrated into the moieties structure of ESA in the presence of ethanol, resulting in a crosslink network structure. Additionally, it formed core–shell spherical nanoparticles with average diameters of ~ 29 nm, having unique properties in the monodispersed and repulsing state (Fig. 1). The morphology of the 3D shape of CET-ANPs speared in the TEM electron micrographs confirms that the NPs were strongly crosslinked, meaning that the CET could interact with the chemical structure of ESA by ionizing interaction through the amino, carboxyl, and intermolecular hydrogen bonds.

#### *Zeta potential and DLS measurements*

The present Zeta potential measurements mainly determined the surface charge of the prepared nanoparticles in solution. Nanoparticles with Zeta potentials in the range of + 20 to − 20 mV could be more stable and have good assembly. In Fig. 2 and Table 2,

**Table 1** Forward and reverse primers of selected genes

| Gene | Forward primer (5′–3′) | Reverse primer (5′–3′) |
|---|---|---|
| *GAPDH* | AGT TCA ACG GCA CAG TCA AG | CGG CCC CAG TTG AAG TTG |
| *Bax* | TCC CCC CGA GAG GTC TTT T | CGG CCC CAG TTG AAG TTG |
| *Bcl2* | TTG GCC CCC GTT GCT T | CGG TTA TCG TAC CCC GTT CTC |
| *Caspase* | TCC TCC TTT GCC AAC ACA CA | TGA CCC ATT TCA TCA CCC ACT |

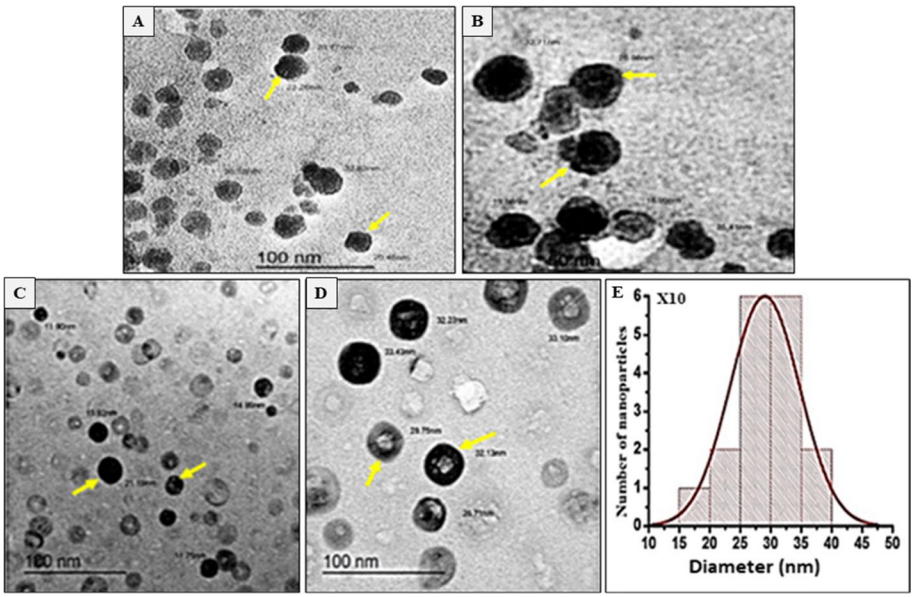


**Fig. 1** **A**, **B** Electron micrographs showing nanospherical shape of ESA-NPS and their size quantification. **C** Electron micrograph showing nanospherical shape of CET-ESA NPs. **D** Magnified portion of **C** confirming nanospherical 3D shape of CET-ANPs with a core–shell crosslink (arrows). **E** Histogram showing numbers and average sizes of CET-ANPs with a range of 15–40 nm detected by TEM

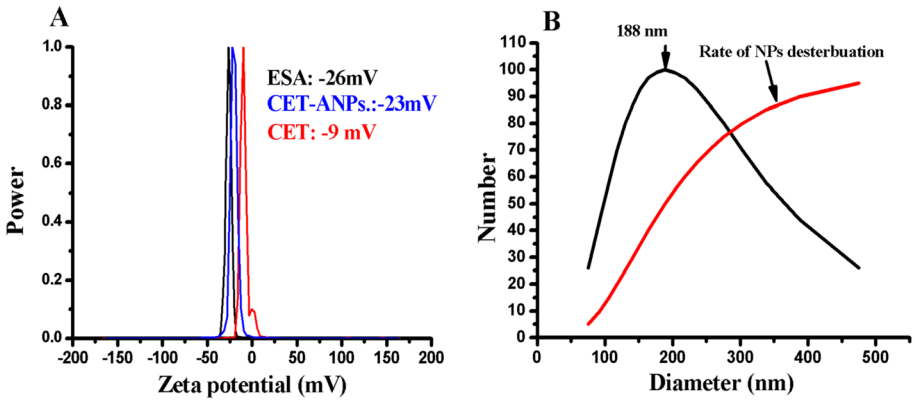


**Fig. 2** Zeta potential and nanosizer showed surface charge of NPs and their mono distributions. Zeta potentials of ESA, CET-ANPs, and CET are **A** − 26, **B** − 23, and **C** − 9 mV, respectively. **B** Diameter of CET-ANPs is 188 nm, and NPs have good rate distribution

**Table 2** Characterization of cetuximab-loaded egg serum albumin nanoparticles

| Drug | Shape | Diameter | Zeta potential | Loading capacity | Encapsulation efficiency |
|---|---|---|---|---|---|
| Cetuximab | Spherical | 15–40 nm | − 23 mV | 66% | 80% |

the Zeta potentials of the ESA and CET-ANPs are − 26 and − 23 mV, respectively, confirming their stability in an aqueous solution, whereas that of the CEF is − 9 mV. The DLS of CET-ANPs in an aqueous solution was estimated at 188 nm.

### *Loading capacity and loading efficiency*

Table 2 shows a summary of the shape, diameter, Zeta potential data, and loading capacity and encapsulation efficiency of CET-ANPs. The data show that the CET-ANPs had efficient drug-loading capacity (66%) and good encapsulation efficiency (80%).

### *UV–Vis spectroscopy and fluorescence spectrophotometry*

The UV visible spectrophotometer showed the characteristic peak of the standard ESA estimated at 280 nm. Also, the fluorescence intensity was observed in the spectrum of the ESA at 342 nm. Similarly, almost the same characteristic peaks were estimated for CET-ANPS and free CET (Fig. 3).

### *Fourier transform infrared spectroscopy (FTIR)*

In the FTIR spectra of the pure ESA powder, the characteristic peaks were observed at 1662 $cm^{-1}$ (–C=O stretching) due to the amide I band and, showing the presence of protein, 1515 $cm^{-1}$ (C–N stretch with the N–H bending mode) due to the amide II band. Similarly, the ESA-NPs show a peak at 1502 $cm^{-1}$, slightly shifting to the lower wavelength due to the N–H bond changes. In the pure CET spectrum, a wide peak occurs at 1649 $cm^{-1}$, resulting from the interaction of CET and ESA CET-ANPs. However, the characteristic peak (1502 $cm^{-1}$) of ESA-NPs disappeared (Fig. 4).

### *SDS-PAGE data*

After encapsulation, the CET antibody was isolated electrically at 115 V from moieties of the ESA-NPs using SDS-PAGE. SDS-PAGE was performed for the pure ESA, pure CET, CET-ANPs, and ESA-NPs. The bands were distributed and separated according to their molecular weights. Figure 5 shows two distinct characteristic bands of the pure CET isolated at 55 and 27 kDa, respectively. These two bands were incorporated among the bands that were isolated from CET-ANPs.

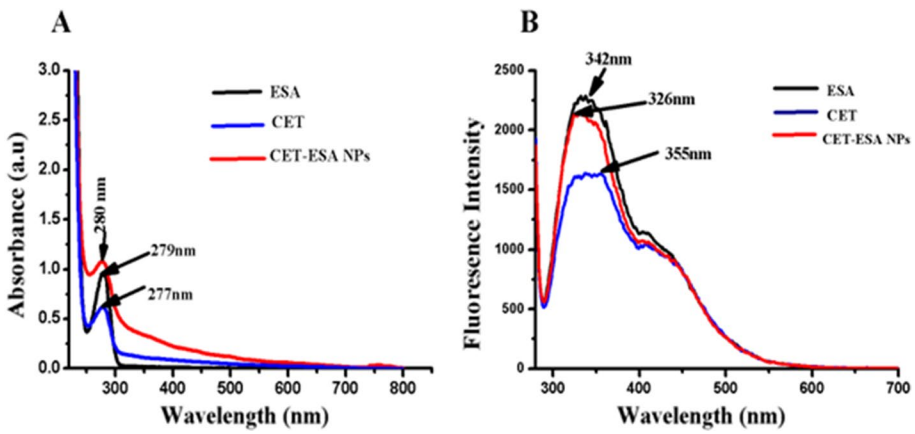


**Fig. 3** UV visible and fluorescence spectrophotometry showed absorbance and fluorescence intensity of ESA, CET, and CET-ANPs. **A** ESA, CET, and CET-ANPs show peaks at 280, 279, and 277 nm, respectively. **B** Fluorescence intensity peaks of ESA, CET-ANPs, and CET/ESA were obtained at 342, 326, and 355 nm, respectively

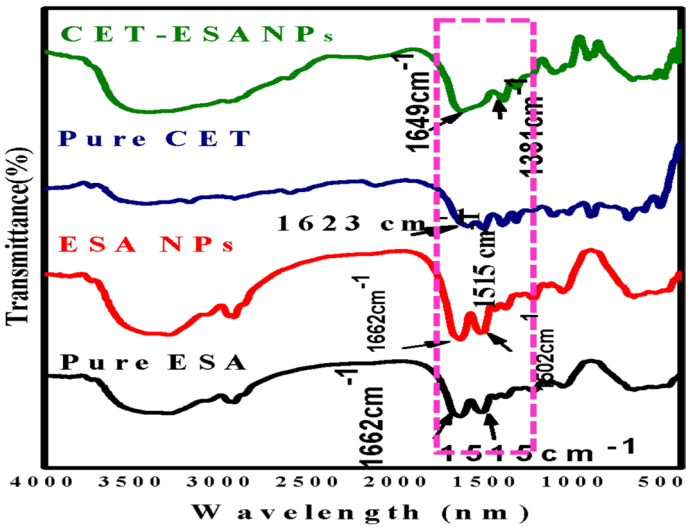


**Fig. 4** FTIR spectra for Pure ESA, ESA-NPs, Pure CET, and CET-ANPs

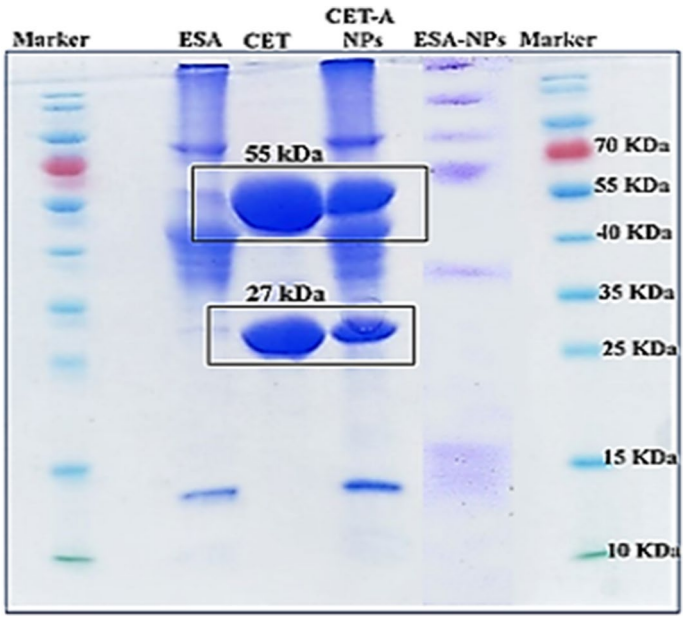


**Fig. 5** SDS-PAGE of pure ESA, pure CET, CET-ANPs, and ESA-NPs showing confirmation of loading of CET moiety with ESA-NPs. Polyacrylamide gels were stained with Coomassie Brilliant Blue

### In vitro assay

Figure 6 shows the MTT assay results of the antitumor effects of CET, ESA, ESA-NPs, and CET-ANPs in the Caco-2 colon cancer cell line. Based on cellular proliferation, Caco-2 cells were significantly inhibited after 24 incubations with 200 µg/ml of CET, ESA-NPs, and CET-ANPs by 45% ± 0.005%, 60% ± 0.005%, and 30% ± 0.01% ($P \leq 0.0001$), respectively. The IC50 values of ESA, CET, ESA-NPs, and CET-ANPs are 287, 230.03, 150.7, and 120 µg/ml, respectively.

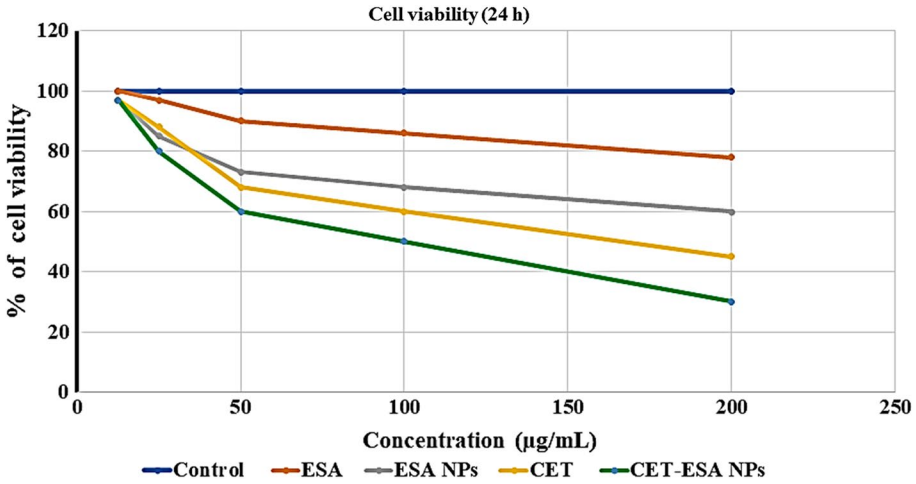


**Fig. 6** Cell viability rate of human colon cancer (Caco-2 cells) incubated with serial concentrations (12.5 to 200 µg/ml) of pure ESA, ESA-NPs, pure CET, and CET-ANPs for 24 h

**Table 3** CI data for nonconstant combination: CET/ESA-NPs

| Dose CET (IC50) | Dose ESA-NPs (IC50) | Effect | CI |
|---|---|---|---|
| 1.0 | 1.0 | 0.96 | 0.60102 |
| 1.0 | 2.0 | 0.80 | 0.07794 |
| 2.0 | 1.0 | 0.49 | **0.01282** |
| 1.0 | 4.0 | 0.89 | 0.27103 |
| 4.0 | 1.0 | 0.68 | 0.05239 |
| 1.0 | 9.0 | 0.54 | 0.08574 |
| 9.0 | 1.0 | 0.53 | 0.03871 |

CI: combination index; effect: mean optical density of treated cells by MTT assay. All combination ratios show a synergistic effect between cetuximab and ESA-NPs, but the ratio 2:1 was the most efficient

### Synergistic cytotoxicity of CET and ESA-NPS combination against Caco-2 cells

Normalized isobolograms and a CI plot were used to identify the interaction type between the CET and the ESA-NPs (CET + ESA-NPs). While all investigated seven combinations reveal a significant synergistically increase in anticancer activities on the Caco-2 cancer cells, although, the 2:1 combination shows the maximum cell death and the lowest CI values (0.01282), as compared with the other combinations (Table 3 and Fig. 7). Initially, the combination of the CET with ESA-NPs enhanced the antitumor activity at a ratio of 2:1 by lowering the survival cells to 49% ± 0.03% ($P \leq 0.001$) (Fig. 8).

### Flow cytometry

#### *Annexin V binding assay for detecting apoptotic cells*

Flow cytometry for apoptotic kit of Annexin V-FITC and IP allowed us to distinguish four cell populations, distributed, respectively, in four different gates as follows: Q1, Q2, Q3, and Q4, respectively (Fig. 9). These four populations are as follows: living (viable) cells (Annexin V-FITC-/IP −), necrotic cells (Annexin V-FITC-/IP +), late apoptotic cells (Annexin V-FITC + /IP +), and early apoptotic cells (Annexin V-FITC + /IP −). The tested agents at IC50 concentrations were applied to Caco-2 cells for 24 h to investigate its possible apoptosis-inducing effect. The data show a

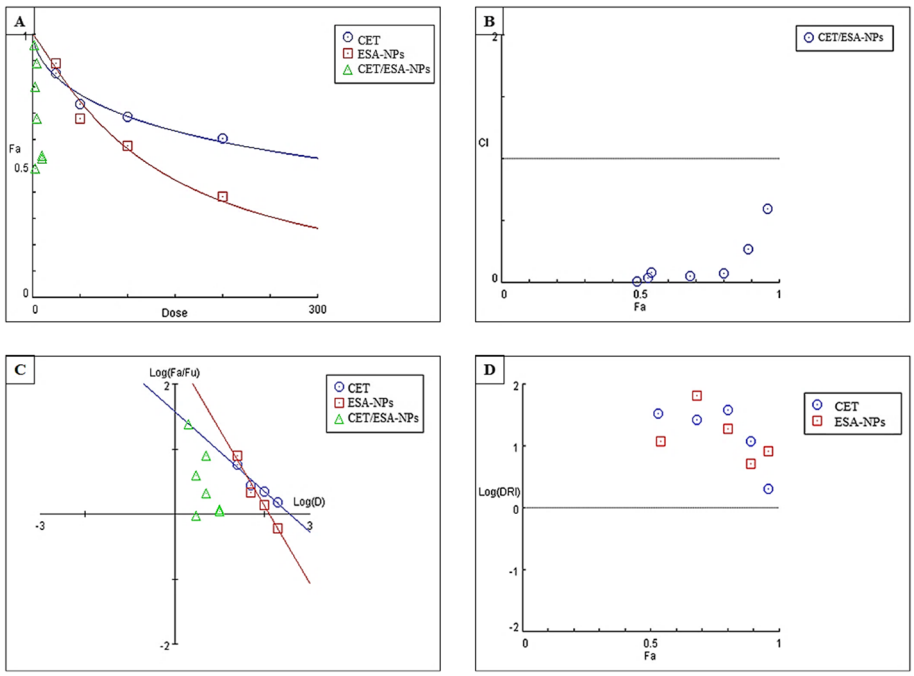


**Fig. 7** Combination index histograms. **A** Combination doses on vertical axes corresponding to both drug levels. **B** Combination index plot displays significant synergistic effects (CI < 1) for all combinations used. **C** Median effect level for both drugs and their combinations. **D** Dose-reduction index log plot for nonconstant combo (CET + ESA-NPs). Fa, initial impact level

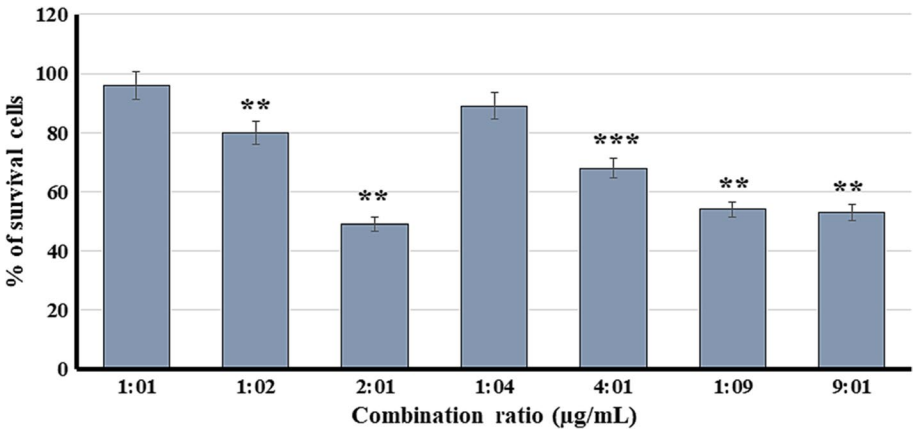


**Fig. 8** Cell viability rate of Caco-2 cells incubated with different combinations of CET + ESA-NPs for 24 h

significant increase in the numbers of the average percentages of late apoptotic cells, as well as the total apoptotic cells (early + late) in Caco-2 cells after exposure to the CET ($P \leq 0.02$), ESA-NPs ($P \leq 0.001$), CET-ANPs ($P \leq 0.0001$), and CET + ESA NPs ($P \leq 0.0001$), as compared to the controls (Table 4). Additionally, the CET alone significantly decreases the average necrotic cell percentages ($P \leq 0.05$), but increases necrosis when administered loaded with ANPs (CET-ANPs) ($P \leq 0.0001$), or as a combined treatment (CET + ESA-NPs) ($P \leq 0.0001$), as compared to the control. In

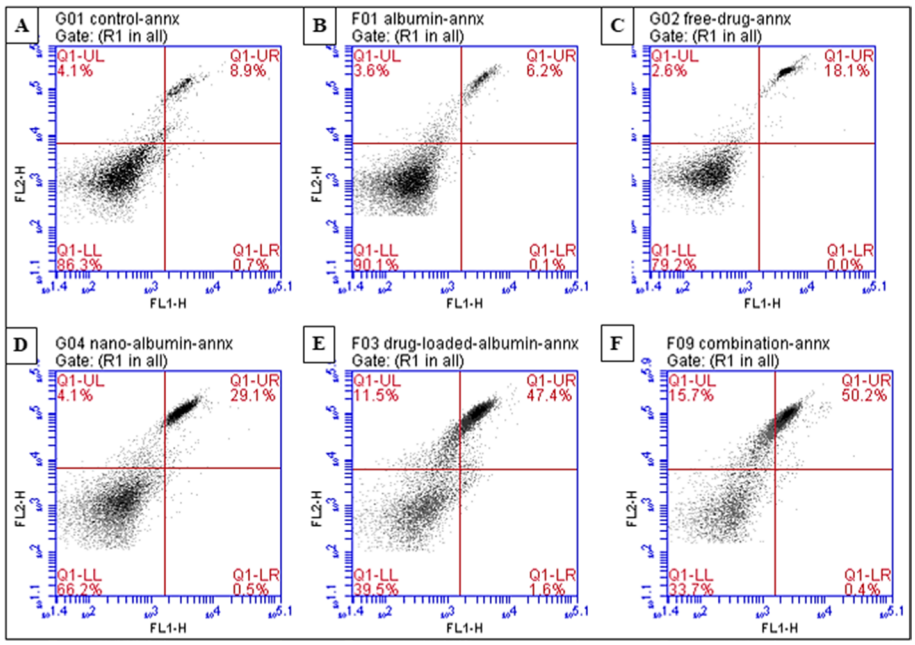


**Fig. 9** Representative flow cytometry plots using Annexin V-FITC/PI staining for apoptosis in Caco-2 cells treated for 24 h. **A** Control, **B** ESA-NPs, **C** pure CET, **D** CET-ANPs, and **E** CET + ESA NPs

**Table 4** Mean percentages of apoptotic, necrotic cells, and cell death

| | Viable cells (% (Gate 1) | Early apoptosis (%) (Gate 4) | Late apoptosis (%) (Gate 3) | Necrosis (%) (Gate 2) | Cell death (%) (apoptosis + necrosis) | Early + Late apoptosis (%) |
|---|---|---|---|---|---|---|
| Control | 84.6 ± 1.8 | 0.8 ± 0.1 | 10.0 ± 1.2 | 4.6 ± 0.5 | 15.4 ± 1.8 | 10.8 ± 1.3 |
| ESA | 90.2 ± 0.0 | 0.1 ± 1.7* | 6.10 ± 0.1 | 3.6 ± 0.1 | 9.80 ± 0.2 | 6.20 ± 1.8 |
| CET | 82.3 ± 3.1 | 0.0 ± 0.0* | 15.3 ± 2.8* | 2.3 ± 0.3* | 17.6 ± 3.1 | 15.3 ± 2.8* |
| ESA-NPs | 66.2 ± 0.3* | 0.5 ± 0.0 | 29.1 ± 0.2** | 4.1 ± 0.1 | 33.7 ± 0.3* | 29.6 ± 0.2** |
| CET-ANPs | 40.0 ± 0.5** | 1.6 ± 0.0** | 46.0 ± 0.7*** | 11.8 ± 0.3*** | 59.4 ± 0.5*** | 47.6 ± 0.1*** |
| CET + ESA-NPs | 35.5 ± 1.0** | 0.3 ± 0.1*** | 48.1 ± 1.9*** | 16.1 ± 0.3*** | 64.5 ± 1.6*** | 48.4 ± 1.9*** |

Data are represented as mean percentages ± SD of three independent experiments. *Significance vs. control at $P < 0.05$; **: Significance *vs.* control at $P < 0.001$; ***Significance vs. control at $P < 0.0001$

contrast, the total cell death (apoptosis + necrosis) also increases significantly after treatment with the CET ($P \leq 0.01$), ESA-NPs ($P \leq 0.001$), CET-ANPs ($P \leq 0.0001$), and CET + ESA-NPs ($P \leq 0.0001$), respectively, as compared to control.

### *Cell cycle analysis*

To determine whether the population growth inhibition observed in the cells is associated with specific changes in cell cycle distribution, the cell cycle analysis using flow cytometry was performed. The average distribution of cell numbers in G0/1, S, and G2/M phases of the cell cycle was estimated in control untreated Caco-2 cells to be 43.1 ± 5.3%, 24.3 ± 1.6%, and 25.7 ± 2.8%, respectively. The treatment of Caco-2 cells with CET, either pure, loaded with (CET-ANPs), or combined with ESA-NPs (CET + ESA-NPs) for 24 h shifts the number of cells in the G0/1 phase (59.53% ± 1.8%, 47.53% ± 0.3%, 40% ± 1.13%, and 41% ± 0.5%), respectively, compared to the control. Also, there is a strong reduction

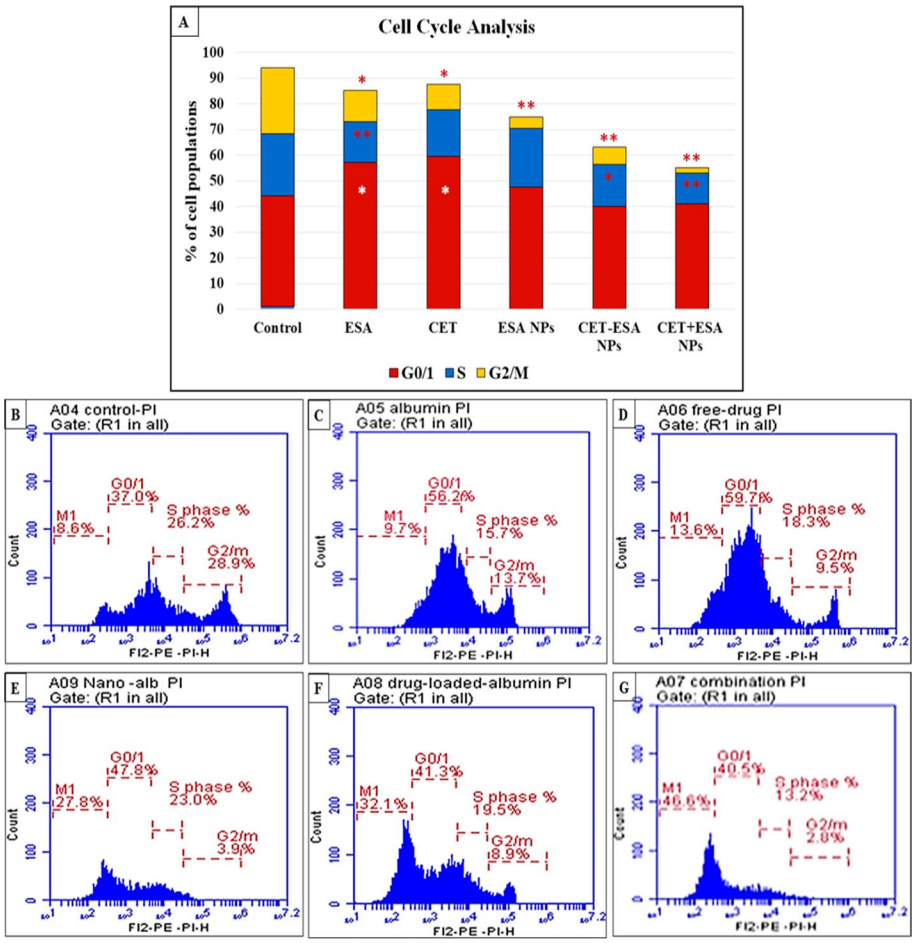


**Fig. 10** **A** Cell cycle analysis data in Caco-2 cells with different treatments showing average percentage numbers of cells at G0/1, S, and G2/M stages of cell cycle. *: significance at $P \leq 0.01$, and *: significance at $P \leq 0.001$. Flow cytometry histograms for cell cycle: **B** untreated control, **C** pure albumin, **D** free CET, **E** ESA-NPs, **F** CET-ANPs, and **G** CET + ESA-NPs combination

in the number of cells exposed to CET + ESA-NPs in the S-phase (12% ± 0.2%, $P \leq 0.001$) compared to the control. In contrast, there is a significant increase in the number of cells exposed to CET-ANPs at the S-phase (40% ± 0.9%, $P \leq 0.01$) compared to the control (Fig. 10).

### Gene expression data analysis

After treatment of the Caco-2 cells with ESA, CET, ESA-NPs, CET-ANPs, or CET + ESA-NPs for 24 h, the gene expressions in the cell apoptotic pathways were investigated, owing to *Bax* and *Bcl-2* having previously been shown to be crucial in mediating the mitochondrial pathway, which leads to the activation of Caspase-9, -3, and -7 (Peng et al. 2018).

The results showed a significant elevation in *Bax* mRNA expression by almost two-fold after treatment with ESA, CET, or CET-ESA NPs ($P \leq 0.01$) (the corresponding figures are: 1.94 ± 0.51, 1.70 ± 0.1, and 1.74 ± 0.12-fold, respectively), and by about 3.3-fold

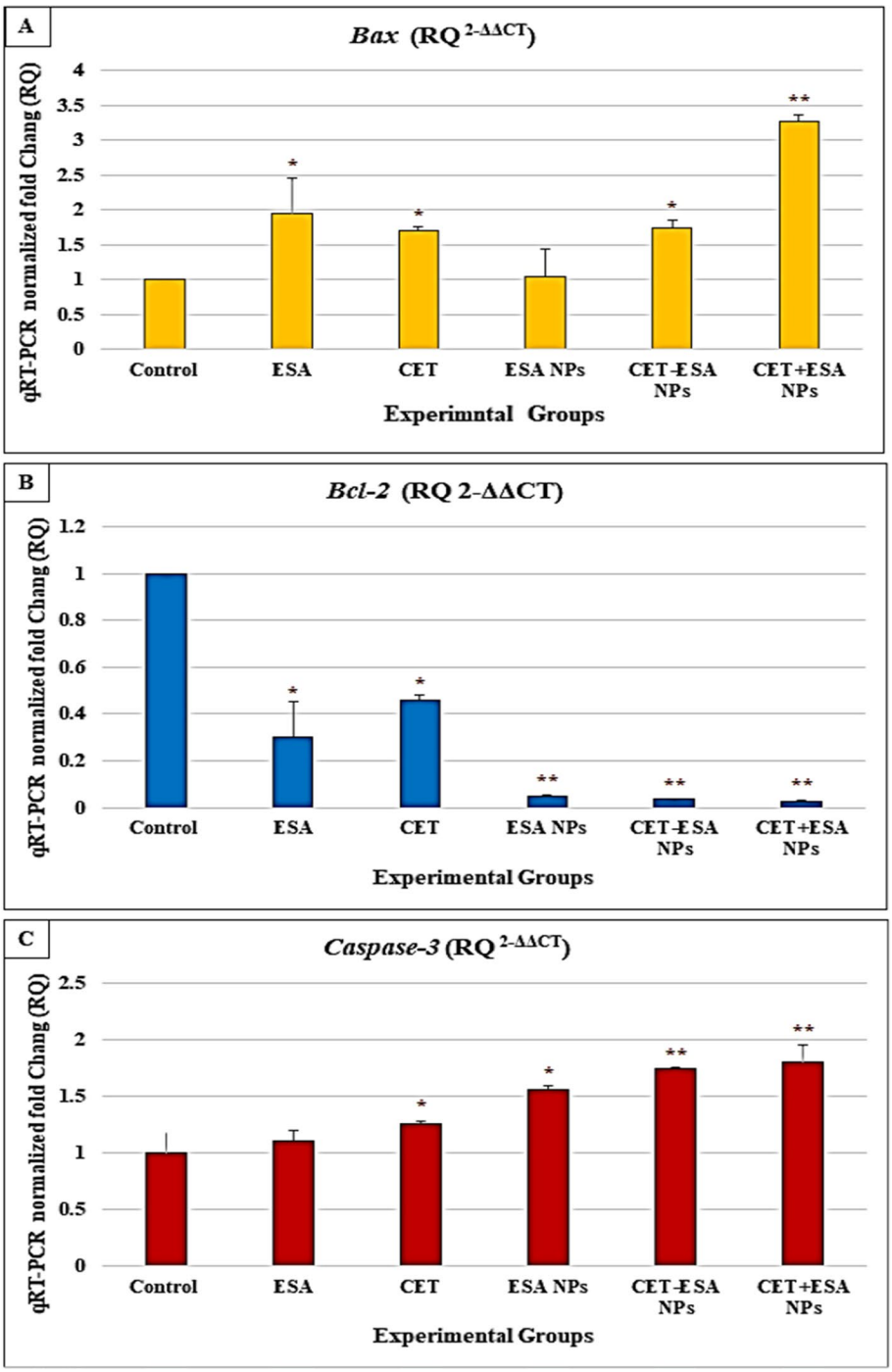


**Fig. 11** Relative fold changes in qRT-PCR mRNA expression levels of **A** *Bax*, **B** *Bcl-2*, and **C** *Caspase-3* genes in Caco-2 cells after 24 h. Data are represented as mean values ± S.D. of three independent experiments after normalization with the *GAPDH* housekeeping gene. *****: Significance *vs*. control at $P \leq 0.01$; ******: significance vs. control at $P \leq 0.0001$

increase ($P \leq 0.0001$) after the combination treatment with CET + ESA NPs, as compared with the control group ($3.27 \pm 0.08$).

In contrast, the mRNA expression of the antiapoptotic *Bcl-2* gene was significantly downregulated after treatment with ESA, CET, ESA-NPs, CET-ESA NPs, and CET + ESA-NPs by 3.33, 2.17, 20, 29.41, and 37.04-fold, respectively. The corresponding figures are $0.3 \pm 0.15$ ($P \leq 0.01$), $0.46 \pm 0.02$ ($P \leq 0.01$), $0.05 \pm 0.01$ ($P \leq 0.0001$), $0.034 \pm 0.001$ ($P \leq 0.0001$), and $0.027 \pm 0.001$ ($P \leq 0.0001$), respectively, as compared with the control (Fig. 11).

Moreover, the mRNA expression of *Caspase-3* was significantly increased by almost 1.5-fold ($P \leq 0.01$) after treatment with CET ($1.3 \pm 0.03$) and ESA-NPs ($1.54 \pm 0.01$), and by an almost twofold increase after treatment with CET-ESA NPs ($1.75 \pm 0.03$), more markedly with the combination treatment ($P \leq 0.0001$) ($1.8 \pm 0.15$).

## Discussion

Recently, in addition to cetuximab, as a monoclonal antibody, and some tyrosine kinase inhibitors having been developed to target EGFR (Harding and Burtness, 2005), albumin nanoparticles, such as bovine serum albumin (BSA) NPs, have emerged as a prospective contender for effective anticancer drug delivery due to their nontoxicity, non-immunogenicity, biodegradability, biocompatibility, and high drug-binding capability. Their use is now a rapidly expanding method to advance cancer therapy (Solanki et al. 2021). Despite its potential efficacy to block the epidermal growth factor and to prevent its phosphorylation, many side effects, however, are gained (Sharifi et al. 2012). For this reason, many efforts have been made to develop new cancer therapies targeting effective genes whose expression occurs in premalignant and malignant lesions (Rosenkranz and Slastnikova 2020).

Herein, CET-loaded ESA-NPs (CET-ESA NPs) showed a spherical shape with a diameter of ~ 29 nm and excellent distribution. Additionally, CET-ANPs exhibited a good surface charge (− 23 mV) and PDI = 0.3 with no aggregation, indicating their excellent repulsive force. Since DLS measures the light scattered from a laser that passes through a colloidal solution and through the analysis, the modulation of the scattered light intensity as a function of time, the hydrodynamic size of particles and particle agglomerates can be determined. Larger particles diffuse slower than smaller particles, and the DLS instrument measures the time dependence of the scattered light to generate a correlation function that can be mathematically linked to the particle size. This may explain the usual slight differences in the nanosize measurements by TEM and DLS (Mahobia et al. 2016). In contrast, it is shown here that the CET can alter the ultimate charge after integrating into the ESA moieties. This trend is in line with the results of the Zeta potential analyses performed by Khoshnamvand et al. (2019), who assessed the stability of the nanoparticles and found a value of − 27.6 mV. The negative Zeta potential value confirms good binding.

CET-loaded ESA-NPs were isolated exactly using the SDS-page after their encapsulation. The isolated CET showed two characteristic bands at 55 and 27 kDa that were exactly similar to the pure CET, confirming the presence of the CET in the structure of the prepared NPs. Similarly, the interaction between the CET and ESA-NPs was

measured by FTIR, showing a wide peak at 1649 $cm^{-1}$, indicating ionic interaction. Also, the usual ESA peak, estimated at 280 nm, was visible on the UV visible spectrophotometer. Also, the spectrum of the fluorescence intensity of the ESA at 342 nm was noticed. Similarly, estimates of the characteristic peaks for the free CET and CET-ANPS were substantially identical. The interaction between the ESA and CET side chains is frequently cited as the cause of this broad range. Several natural nanoparticles exhibited two unique bands at 336 and 454 nm, which are linked to specific compounds, according to Barbieri et al. (2020).

To better understand the cytotoxicity of CET-ESA NPs on Caco-2 cell lines, all materials used in fabrication were subjected to MTT assay with serial concentrations (12.5, 25, 50, 100, and 200 µg/ml) for 24 h. CET-ANPs expressed significant inhibition of $P \leq 0.001$ to the growth of Caco-2 by (85% ± 0.02%, 84% ± 0.01%, 69% ± 0.01%, 60% ± 0.01%, 43% ± 0.01%), respectively. Increasingly, CET-combined ESA-NPs showed a highly significant effect on Caco-2. This combination could boost the anticancer activity of available drugs while suppressing their unwanted side effects after incubation for 48 h (Park et al. 2014). Such an experiment provided a better understanding of the synergistic effect of the CET and ESA-NPs. Recently, liposomal and micellar cytostatics or albumin-based nanoparticles have shown less adverse effects and are more effective than "free" medications, according to clinical research and licensed anticancer medical treatments (Kopeckova et al. 2019). Almost similar results were obtained by Pham et al. (2021). They loaded human serum albumin (HSA) nanoparticles with paclitaxel (PTX) via nanoparticle albumin-bound technology and pooled them with anti-PD-L1 monoclonal antibodies through a pH-sensitive linker for targeting and immune response activation. To increase gemcitabine's therapeutic index against MCF-7 cells, we have recently employed gemcitabine against MCF-7 cells by loading it onto albumin nanoparticles and coating it with chitosan (Salim et al. 2022). We suggested that the modified ANPs coated with chitosan could be used as a potential nanomatrix for gemcitabine delivery and targeting.

Here, utilizing Chou and Talalay's CI equation (CI = 1), it was discovered that all combinations of CET + ESA-NPs had a general synergistic colon cancer-inhibiting effect. The CI ratios of the 1:2 combination are regarded as particularly low compared to the other combination regimens used here, with every other combination ratio evaluated here having a synergistic impact, demonstrating that CET and ESA-NPs had a strong interaction, a potentially strong and selective toxic effect of the combination synergism on colon cancer cells is indicated. Doxorubicin and OSMI-1 (an OGT inhibitor) have recently been shown to work in synergy to reduce the IC50 value of Doxorubicin and kill cancer cells (Makwana et al. 2020). Also, the antitumor synergy has been demonstrated for many chemotherapeutic drugs and adjuvant therapy, such as the HDAC inhibitors vorinostat, 17-DMAG, abacavir, sorafenib, and telomerase inhibitors abacavir. Also, it has been demonstrated for sorafenib alone, together, or in combination with doxorubicin (Dumont et al. 2014).

The mechanism by which the CET caused cell cytotoxicity was studied using flow cytometry. Annexin V-FITC-/IP- was used to detect the population of early apoptosis, late apoptosis, and necrotic cells. The apoptotic cells were significantly increased in CET-ANPs and CET + ESA-NPs by 46% ± 0.6% and 48% ± 1.8% at $P \leq 0.0001$, respectively. Furthermore, the necrotic cells were also significantly increased in CET-ANPs and

CET + ESA-NPs by 11% ± 0.2% and 16 ± 0.32% at $P \leq 0.0001$, respectively. This information supports the work of Visentini et al. (2020). They postulated that conjugated linoleic acid delivery systems were attractive nanosupplements for developing new functional foods and excipients for colon cancer prevention and treatment. A recent study by Li et al. (2021) using the cellular uptake test has shown that 5FU-ABX-encapsulated BLDH (BLDH/5FU-ABX) nanoparticles were effectively internalized by the colorectal cancer cell (HCT-116), synergistically inducing apoptosis of colon cancer cells. This research lends support to the current mechanism of action. Additionally, Thao et al. (2016) highlighted a new nanoparticle formulation containing HSA for the simultaneous administration of the anticancer drug, doxorubicin (Dox), and tumor necrosis factor-related apoptosis-inducing ligand to promote an apoptotic response in vitro and in vivo, in line with our present suggested mechanism of action.

Moreover, the expression of antiapoptotic *Bcl-2* gene was significantly ($P \leq 0.001$) inhibited by ~ 0.5 ± 0.1, 0.43 ± 0.02, 0.04 ± 0.01, 0.035 ± 0.001, and 0.025 ± 0.001-fold compared with the control group by ~ 0.5 ± 0.1, 0.43 ± 0.02, 0.04 ± 0.01, 0.035 ± 0.001, and 0.025 ± 0.001-fold in Caco-2 treated by the ESA, CET, ESA-NPs, CET-ESA NPs, and CET + ESA-NPs, respectively. El-Deeb et al. (2015) have shown that nanoparticles made from honeybee extract inhibited colon cancer by 60% by reducing the expression of *Bcl-2*. Also, the expression of proapoptotic genes, such as *Bax*, and *Caspase-3* with the ESA, CET, ESA-NPs, and CET-ANPs treatment were upregulated by 1.06 ± 0.02, 1.6 ± 0.02, 1.74 ± 0.02, and 1.94 ± 0.01-fold, respectively, and 1.2 ± 0.01, 1.25 ± 0.02, 1.55 ± 0.03, and 1.72 ± 0.02-fold, respectively. Li et al. (2022) showed that the toxicity mechanism increased apoptosis induction by raising the expression of the *Bax* and *Caspase-3* genes when using platinum nanospheres loaded with 5-fluorouracil (FLU) and bovine albumin against colon tumor xenografts in vivo in comparison to the free drug.

The phases of cell cycle division frequently arising during replication were differentiated using PI. The result, while there was a real reduction in G2/M by 7% ± 1.7% compared to the control (25.7% ± 2.8%) (Peng et al. 2018), showed that CET-ANPs showed a significant increase in the number of cells conducted to the S-phase (40% ± 0.006%) compared to the control (24% ± 1.6%). Recently, 9-hydroxystearic acid combined with histone deacetylases (HDAC1) has been shown to cause cell growth inhibition and differentiation in the HT-29 colon cell line. The treatment caused a G0/G1 phase cell cycle arrest and activation of the $p21^{WAF1}$ gene. Also, the 9-hydroxystearic acid treatment alone has been shown to arrest the S-phase cell cycle (25% increase as compared to the control) with respect to the induction of cell death (Busi et al. 2019). In contrast, and damaging both mitochondria and causing apoptosis, according to mechanistic investigations on HCT116 colon cancer cells (Icsel et al. 2018) the neutral and cationic saccharinate complexes cause the S-phase cell cycle arrest and excessive formation of reactive oxygen species. Moreover, Terzuoli et al. (2017) showed that cetuximab combined with hydroxytyrosol caused a significant delay in the cell cycle movement in colon cancer cells.

## Conclusion

Herein, it was found that using our modified ESA-NPs with cetuximab improved the therapeutic index of cetuximab against Caco-2 colon cancer cells. The structure of CET-ESA NPs improved the particle cell penetration and increased cellular internalization, resulting in more potent cytotoxicity and apoptotic effects on Caco-2 cells. The antitumor activity and apoptotic effect of CET-ANPs outperformed the effect of pure CET. These findings indicate promising therapeutic approaches of CET-ANPs to be used later in vivo.

**Abbreviations**

| | |
|---|---|
| ANOVA | Analysis of variance |
| CET | Cetuximab |
| CET-ANPs | Cetuximab-loaded egg serum albumin nanoparticles |
| CET + ESA-NPs | Cetuximab combination with egg serum albumin nanoparticles |
| DMSO | Dimethylsulfoxide |
| DLS | Dynamic light scattering |
| ESA | Egg serum albumin |
| EGFR | Epidermal growth factor receptor |
| FTIR | Fourier transform infrared |
| kDa | Kilo Dalton |
| KBr | Potassium bromide |
| NPs | Nanoparticles |
| NSCLC | Non-small cell lung cancer |
| OVA | Ovalbumin |
| PI | Propidium iodide |
| RT-PCR | Real-time-polymerase chain reaction |
| SD | Standard deviation |
| SDS-PAGE | Sodium dodecyl sulfate–polyacrylamide gel electrophoresis |
| TEM | Transmission electron microscope |
| UV–Vis | Ultraviolet visible |

**Acknowledgements**

The authors wish to thank the Egyptian Knowledge Bank (EKB), at the Specialized Presidential Council for Education and Scientific Research, Egypt, for its aid of the scientific English correction for this paper. For their gracious support and technical assistance, the authors like to thank all the members of the Research Laboratory of Molecular Carcinogenesis at the Zoology Department, Faculty of Science, Tanta University, Egypt.

**Author contributions**

ES set the conception and the experimental design, was a major contributor to writing the manuscript and performed the molecular analysis, flow cytometrical cell analysis and data interpretation for nanoparticles; AM performed the nanoparticle preparation and contributed to writing the manuscript. FA has contributed to the physics of the nanoparticles' preparation and characterization, and revision of the manuscript. NH contributed to the preparation and characterization of the nanoparticles and to the text writing. YA contributed to the experimental design, physics of the nanoparticles' preparation and characterization, and revision of the text. All authors have agreed to be personally accountable for their contributions. And to ensure that any questions about the accuracy or integrity of any part of the work, even if they were not personally involved, are appropriately investigated, resolved, and the resolution documented in the literature. All authors read and approved the final manuscript.

**Funding**

Open access funding provided by The Science, Technology & Innovation Funding Authority (STDF) in cooperation with The Egyptian Knowledge Bank (EKB). The authors report that they got no financial support from any funding source for the study design, data collection, analysis, interpretation. International English correction of this paper was funded by the Egyptian Knowledge Bank (EKB) of the Specialized Presidential Council for Education and Scientific Research, Egypt.

## Declarations

**Ethics approval and consent to participate**

Not applicable.

**Consent for publication**

Not applicable.

**Competing interests**

There are no competing interests declared by the authors.

Received: 5 November 2022 Accepted: 29 December 2022
Published online: 16 January 2023

**References**

Abou-Zeid AA, Khafagy W, Marzouk DM, Alaa A, Mostafa I, Ela MA (2002) Colorectal cancer in Egypt. Dis Colon Rectum 45:1255–1260. https://doi.org/10.1007/s10350-004-6401-z

Ali EMM, Elashkar AA, El-Kassas HY, Salim EI (2018) Methotrexate loaded on magnetite iron nanoparticles coated with chitosan: Biosynthesis, characterization, and impact on human breast cancer MCF-7 cell line. Int J Biol Macromol 120(Pt A):1170–1180. https://doi.org/10.1016/j.ijbiomac.2018.08.118

Barbieri D, Gabriele M, Summa M, Colosimo R, Leonardi D, Domenici V, Pucci L (2020) Antioxidant, nutraceutical properties, and fluorescence spectral profiles of bee pollen samples from different botanical origins. Antioxidants (basel) 9(10):1001. https://doi.org/10.3390/antiox9101001

Busi A, Aluigi A, Guerrini A, Boga C, Sartor G, Calonghi N, Sotgiu G, Posati T, Corticelli F, Fiori J, Varchi G, Ferroni C (2019) Unprecedented behavior of (9 R)-9-hydroxystearic acid-loaded keratin nanoparticles on cancer cell cycle. Mol Pharm 16(3):931–942. https://doi.org/10.1021/acs.molpharmaceut.8b00827

Chou TC, Talalay P (1984) Quantitative analysis of dose-effect relationships: the combined effects of multiple drugs or enzyme inhibitors. Adv Enzyme Regul 22:27–55. https://doi.org/10.1016/0065-2571(84)90007-4

Dumont S, Yang D, Dumont A, Reynoso D, Blay J, Trent J (2014) Targeted polytherapy in small cell sarcoma and its association with doxorubicin. Mol Oncol 8(8):1458–1468. https://doi.org/10.1016/j.molonc.2014.05.016

El-Bolkainy T, Sakr M, Nouh A, El-Din N (2006) A comparative study of rectal and colonic carcinoma: demographic, pathologic and TNM staging analysis. J Egypt Natl Cancer Inst 18:258–263

El-Deeb NM, El-Sherbiny IM, El-Aassara MR, Hafez EE (2015) Novel trend in colon cancer therapy using silver nanoparticles synthesized by honey bee. J Nanomed Nanotechnol 6(2):265. https://doi.org/10.4172/2157-7439.1000265

Feng M, Zhong LX, Zhan ZY, Huang ZH, Xiong JP (2017) Enhanced antitumor efficacy of resveratrol-loaded nanocapsules in colon cancer cells: physicochemical and biological characterization. Eur Rev Med Pharmacol Sci 2:375–382

Ferrado JB, Perez AA, Ruiz MC, León IE, Santiago LG (2020) Chrysin-loaded bovine serum albumin particles as bioactive nanosupplements. Food Funct 11(7):6007–6019. https://doi.org/10.1039/d0fo00299b

Fogh J (1986) Human tumor lines for cancer research. Cancer Invest 4(2):157–184. https://doi.org/10.3109/07357908609038260

Hanafy NAN, Leporatti S, El-Kemary M (2020) Mucoadhesive curcumin crosslinked carboxy methyl cellulose might increase inhibitory efficiency for liver cancer treatment. Mater Sci Eng C Mater Biol Appl 116:111119. https://doi.org/10.1016/j.msec.2020.111119

Harding J, Burtness B (2005) Cetuximab: an epidermal growth factor receptor chemeric human-murine monoclonal antibody. Drugs Today (barc) 41(2):107–127. https://doi.org/10.1358/dot.2005.41.2.882662

Hatanpaa KJ, Burma S, Zhao D, Habib AA (2010) Epidermal growth factor receptor in glioma: signal transduction, neuropathology, imaging, and radioresistance. Neoplasia 12(9):675–684. https://doi.org/10.1593/neo.10688

Icsel C, Yilmaz VT, Aygun M, Cevatemre B, Alper P, Ulukaya E (2018) Palladium(ii) and platinum(ii) saccharinate complexes with bis(diphenylphosphino)methane/ethane: synthesis, S-phase arrest and ROS-mediated apoptosis in human colon cancer cells. Dalton Trans 47(33):11397–11410. https://doi.org/10.1039/c8dt02389a

Karami K, Hosseini-Kharat M, Sadeghi-Aliabadi H, Lipkowski J, Mirian M (2014) In vitro cytotoxicity studies of palladacyclic complexes containing the symmetric diphosphine bridging ligand. Studies of their interactions with DNA and BSA. Eur J Med Chem 73:8–17. https://doi.org/10.1016/j.ejmech.2013.11.042

Khaliq B, Falke S, Saeed Q, Bilal M, Munawar A, Ali A, Baermann G, Athar HU, Mahmood S, Betzel C, Ali Q, Akrem A (2021) Eruca sativa seed napin structural insights and thorough functional characterization. Sci Rep 11(1):24066. https://doi.org/10.1038/s41598-021-02174-6

Khamis AAA, Ali EMM, El-Moneim MAA, Abd-Alhaseeb MM, El-Magd MA, Salim EI (2018) Hesperidin, piperine and bee venom synergistically potentiate the anticancer effect of tamoxifen against breast cancer cells. Biomed Pharmacother 105:1335–1343. https://doi.org/10.1016/j.biopha.2018.06.105

Khoshnamvand M, Huo C, Liu J (2019) Silver nanoparticles synthesized using Allium ampeloprasum L. leaf extract: characterization and performance in catalytic reduction of 4-nitrophenol and antioxidant activity. J Mol Struct 1175:90–96

le Thao Q, Byeon HJ, Lee C, Lee S, Lee ES, Choi YW, Choi HG, Park ES, Lee KC, Youn YS (2016) Doxorubicin-Bound Albumin Nanoparticles Containing a TRAIL Protein for Targeted Treatment of Colon Cancer. Pharm Res 33(3):615–626. https://doi.org/10.1007/s11095-015-1814-z

Li L, Qian Y, Sun L, Han FY, Zhang R, Wang PY, Xu ZP (2021) Albumin-stabilized layered double hydroxide nanoparticles synergized combination chemotherapy for colorectal cancer treatment. Nanomedicine 34:102369. https://doi.org/10.1016/j.nano.2021.102369

Li H, Sun Y, Gao LL, Tang YF, Zhao Z (2022) The treatment of human colon xenografts tumor in mice with platinum nanosphere-5-fluorouracil-bovine albumin. J Biomed Nanotechnol 18(3):778–787. https://doi.org/10.1166/jbn.2022.3271

Mahobia S, Bajpai J, Bajpai AK (2016) An in-vitro investigation of swelling controlled delivery of insulin from egg albumin nanocarriers. Iran J Pharm Res 15(4):695–711

Makwana V, Dukie APS-A, Rudrawar S (2020) Investigating the impact of OGT inhibition on doxorubicin-and docetaxel-induced cytotoxicity in PC-3 and WPMY-1 cells. Int J Toxicol 39(6):586–593. https://doi.org/10.1177/1091581820948433

Park HK, Lee JE, Lim J, Jo D-E, Park S-A, Suh P-G, Kang BH (2014) Combination treatment with doxorubicin and gamitrinib synergistically augments anticancer activity through enhanced activation of Bim. BMC Cancer 14:431. https://doi.org/10.1186/1471-2407-14-431

Peng F, Zhang H, Du Y, Tan P (2018) Cetuximab enhances cisplatin-induced endoplasmic reticulum stress-associated apoptosis in laryngeal squamous cell carcinoma cells by inhibiting expression of TXNDC5. Mol Med Rep 17(3):4767–4776. https://doi.org/10.3892/mmr.2018.8376

Pham LM, Poudel K, Ou W, Phung CD, Nguyen HT, Nguyen BL, Karmacharya P, Pandit M, Chang JH, Jeong JH, Ku SK, Yong CS, Choi HG, Kim JO (2021) Combination chemotherapeutic and immune-therapeutic anticancer approach via anti-PD-L1 antibody conjugated albumin nanoparticles. Int J Pharm 605:120816. https://doi.org/10.1016/j.ijpharm.2021.120816

Rosenkranz AA, Slastnikova TA (2020) Epidermal growth factor receptor: key to selective intracellular delivery. Biochemistry Moscow 85:967–993. https://doi.org/10.1134/S0006297920090011

Salim EI, Abd El Khalik EAM, Shalaby TI, Ali EMM (2022) Synthesis, characterisation and enhanced apoptotic effect of gemcitabine-loaded albumin nanoparticles coating with chitosan. Arch Physiol Biochem 128(4):970–978. https://doi.org/10.1080/13813455.2020.1742165

Sharifi S, Behzadi S, Laurent S, Forrest ML, Stroeve P, Mahmoudi M (2012) Toxicity of nanomaterials. Chem Soc Rev 41:2323–2343. https://doi.org/10.1039/c1cs15188f

Solanki R, Rostamabadi H, Patel S, Jafari SM (2021) Anticancer nano-delivery systems based on bovine serum albumin nanoparticles: A critical review. Int J Biol Macromol 193(Pt A):528–540. https://doi.org/10.1016/j.ijbiomac.2021.10.040

Štulhofer Buzina D, Martinac I, Ledić Drvar D, Čeović R, Bilić I, Marinović B (2016) Adverse reaction to cetuximab, an epidermal growth factor receptor inhibitor. Acta Dermatovenerol Croat 24(1):70–72

Sung H, Ferlay J, Siegel RL, Laversanne M, Soerjomataram I, Jemal A, Bray F (2021) Global Cancer Statistics 2020: GLOBOCAN estimates of incidence and mortality Worldwide for 36 Cancers in 185 Countries. CA Cancer J Cin 73(3):209–249. https://doi.org/10.3322/caac.21660

Terzuoli E, Nannelli G, Frosini M, Giachetti A, Ziche M, Donnini S (2017) Inhibition of cell cycle progression by the hydroxytyrosol-cetuximab combination yields enhanced chemotherapeutic efficacy in colon cancer cells. Oncotarget 8(47):83207–83224. https://doi.org/10.18632/oncotarget.20544

Veruttipong D, Soliman AS, Gilbert SF, Blachley TS, Hablas A, Ramadan M, Rozek LS, Seifeldin IA (2012) Age distribution, polyps and rectal cancer in the Egyptian population-based cancer registry. World J Gastroenterol 18(30):3997–4003. https://doi.org/10.3748/wjg.v18.i30.3997

Visentini FF, Perez AA, Baravalle ME, Renna MS, Ortega HH, Santiago LG (2020) In vitro gastrointestinal digestion and cytotoxic effect of ovalbumin-conjugated linoleic acid nanocomplexes. Food Res Int 137:109381. https://doi.org/10.1016/j.foodres.2020.10938

Ye Z, Zhang Y, Liu Y, Liu Y, Tu J, Shen Y (2021) EGFR targeted cetuximab-valine-citrulline (vc)-doxorubicin immunoconjugates-loaded bovine serum albumin (BSA) nanoparticles for colorectal tumor therapy. Int J Nanomed 16:2443. https://doi.org/10.2147/IJN.S289228

Kis AM, Macasoi I, Paul C, Radulescu M, Buzatu R, Watz CG, Cheveresan A, Berceanu D, Pinzaru I, Dinu S, Manea A, Poenaru M, Borza C, Dehelean CA (2022) Methotrexate and Cetuximab-Biological Impact on Non-Tumorigenic Models: In Vitro and In Ovo Assessments. Medicina. 58(2):167. https://doi.org/10.3390/medicina58020167.

Kopeckova K, Eckschlager T, Sirc J, Hobzova R, Plch J, Hrabeta J, Michalek J. Nanodrugs used in cancer therapy (2019). Biomed Pap Med Fac Univ Palacky Olomouc Czech Repub 163(2):122–131. https://doi.org/10.5507/bp.2019.010.

## Publisher's Note

Springer Nature remains neutral with regard to jurisdictional claims in published maps and institutional affiliations.

**Ready to submit your research? Choose BMC and benefit from:**

- fast, convenient online submission
- thorough peer review by experienced researchers in your field
- rapid publication on acceptance
- support for research data, including large and complex data types
- gold Open Access which fosters wider collaboration and increased citations
- maximum visibility for your research: over 100M website views per year

**At BMC, research is always in progress.**

**Learn more** biomedcentral.com/submissions